Aalborg Universitet

Operation Mode Transition Technique of Flexible Modulation Scheme for Single-phase Transformerless PV Inverters

Zhongting Tang, Ariya Sangwongwanich, and Frede Blaabjerg

AAU Energy, Aalborg University, Aalborg 9220, Denmark

E-mails: zta@et.aau.dk, ars@energy.aau.dk, fbl@et.aau.dk

Abstract—The advanced modulation scheme with reactive power injection is preferred in single-phase transformerless PV inverters, (e.g., H5, H6, and HERIC), which can achieve high efficiency as well as flexible power control capability. Considering the turn-on and turn-off periods of real semiconductor devices, the deadtime is indispensable between the switching of bridge switches to avoid the short-through phenomenon. The deadtime should be inserted into not only the switching state transition (in one switching cycle) but also the operation mode transition (in one grid cycle). Among, the deadtime insertion during the operation mode transition always causes current distortions at the AC voltage zero-cross point, or even fails the mode transition. Thus, this paper proposes an improved switching mode transition strategy to ensure the exact mode transition and the high power quality of PV inverters. Simulation and experiments have been carried out on a grid-connected transformerless PV inverter prototype, verifying the excellent performance on the power quality of the proposed technique.

Index Terms—Modulation, operation transition, current distortion, power quality, PV transformerless inverter

I. INTRODUCTION

Solar energy is occupying the share of power systems and distribution systems worldwide at an unprecedented speed, which is expected to provide 35% of global electricity generation by 2050 [1]. The solar photovoltaic (PV) systems are based on inverters, where relevant techniques have been researched and developed correspondingly, e.g., topologies, modulation methods, control, and grid-connected strategies [2]–[4]. Single-phase transformerless inverters perform extremely well in low- and medium-power photovoltaic (PV) energy generation systems, e.g., smart residential PV systems, and self-consumption PV systems [4]. Without physical transformers, they can have good performance in terms of high efficiency, high compactness as well as low leakage current [5]. The representative topologies are the H5 inverter, H6 topologies (e.g., DC-decoupled H6 and AC-decoupled H6 inverters), and the highly efficient and reliable inverter concept (HERIC) [6], as shown in Fig. 1 (a)-(c), respectively.

The high penetration of PV Power requires new "smart" capabilities of the inverters in addition to their primary functionality of active power generation [2]. The grid integration should not only alleviate the fluctuation of solar energy but
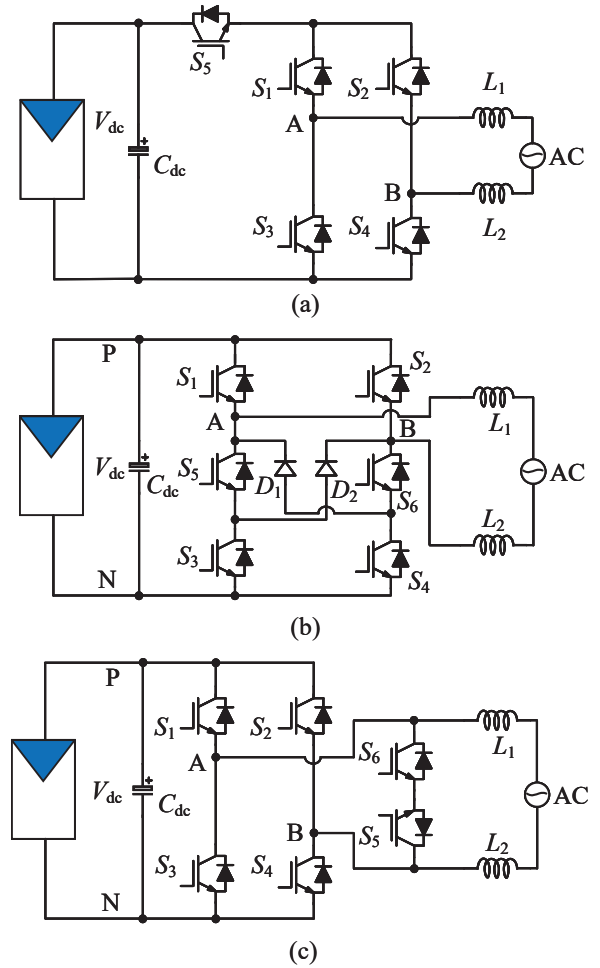
Fig. 1. Typical transformerless single-phase PV inverters, (a) H5 inverter, (b) AC-decoupled H6 inverter, and (c) HERIC inverter.

also support the grid voltage as required and even under abnormal conditions (e.g., low-voltage ride-through (LVRT)). Therefore, apart from the requirement on the leakage current for the grid-connected PV inverters, many standards released in recent years have more advanced demands on flexible power control function, i.e., IEEE Std. 1547-2018 [7]. To achieve reactive power injection capability as well as ensure

a low leakage current, several typical modulation methods have been developed [8]–[10]. For example, the bipolar pulse width modulation (PWM) method for the H-bridge inverter is adopted to achieve low leakage current and the reactive power injection capability, where the efficiency is compromised. To alleviate efficiency, [8] proposed an improved modulation method with combined unipolar and bipolar PWMs. Besides, an improved modulation method has been proposed for single-phase transformerless inverters (i.e., mainly explored in H5 and HERIC inverters) in [9], which has been extended for all the transformerless PV inverters [4], [10].

Except for the reactive power injection, the power quality is also an important and basic requirement when performing the modulation methods. However, the deadtime in reality impacts the power quality a lot, which is a mandatory requirement in modulation schemes during the switching of the power devices on one bridge leg [11]. The deadtime in the switching interval (switching cycle) leads to the voltage reducing or increasing [12], while the deadtime during the operation mode transition (i.e., the operation mode transition from the positive half-cycle to the negative half-cycle) causes the current distortion near the voltage zero-cross point [13], or even fails the mode transition. Many studies focus on the compensation for the zero-cross distortion, where a precise compensation method is proposed in the modulation with the reactive power injection to eliminate the deadtime effects in [13]. Nevertheless, less research discusses the transition process of the operation modes, which is impacted by the deadtime, the voltage and current detection errors.

Therefore, this paper proposes an improved operation mode transition strategy, which is demonstrated in a typical transformerless single-phase PV inverter, i.e., the HERIC inverter (see Fig. 1(c)). The rest of the paper is arranged as the following. Section II presents the specific operation states of the advanced modulation method with reactive power injection based on the HERIC inverter, and follows the distortion analysis due to the deadtime between the operation mode transition. Correspondingly, a completed process of the operation mode transition strategy has been proposed in Section III, where the switching states and transition schemes have been detailed. Then, Section IV validates the effectiveness of the proposed mode transition strategy. Finally, the conclusion gives in Section V.

II. MODULATION SCHEME WITH REACTIVE POWER INJECTION

A. Operation mode description

This paper takes the HERIC inverter for example to analyze the advanced modulation method and its transition issue due to the deadtime. As depicted in Fig. 1 (c), the HERIC inverter includes six switches, S_{1-6} (i.e, IGBTs with paralleled diodes), two symmetrical AC inductor filters $L_{1,2}$, and one DC-link capacitor C_{dc}. Fig. 2 (a) shows the modulation scheme with the reactive power injection for the HERIC inverter (i.e., shown in Fig. 1(c)), where v_{ref} is the modulation signal generated from the controller, and i_{ref} is the reference AC output current. As
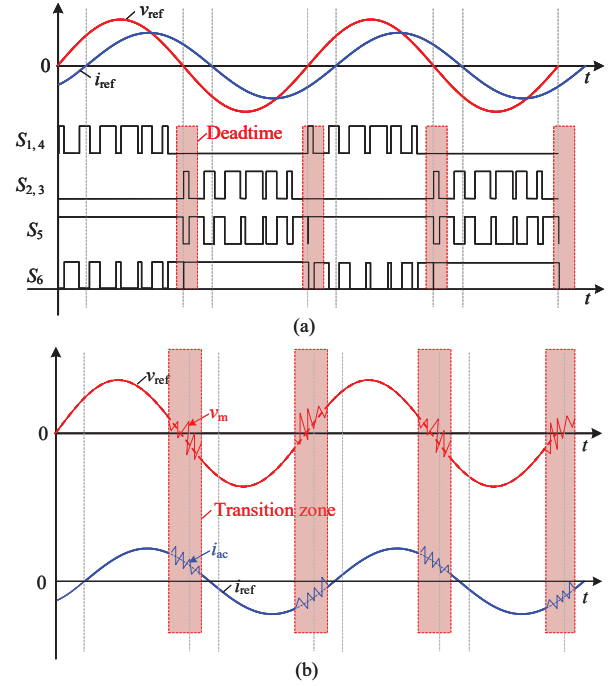

Fig. 2. Modulation scheme of the HERIC inverter with reactive power injection, (a) switching principle and (b) distortion during the mode transition.

TABLE I
SWITCHING STATE OF THE IMPROVED MODULATION SCHEME WITH DEADTIMES FOR THE HERIC INVERTER.

v_{ref}	Mode	S_1	S_2	S_3	S_4	S_5	S_6	v_{AB}
P_M	+Dt	−	−	−	−	+	−	0
	Pv	+	−	−	+	−	+	$+v_{AB}$
	+Dt	−	−	−	−	+	−	0
	Zv	−	−	−	−	+	+	0
OFF	Dt	−	−	−	−	−	−	$\pm v_{AB}$
N_M	−Dt	−	−	−	−	−	+	0
	Nv	−	+	+	−	−	+	$-v_{AB}$
	−Dt	−	−	−	−	−	+	0
	Zv	−	−	−	−	+	+	0

shown in Fig. 2 (a), the modulation scheme mainly includes two operation modes, i.e., positive half-cycle mode (P_M) and negative half-cycle mode (N_M). The detailed switching states are presented in Table I, where the operation mode of P_M includes the positive voltage switching state P_v, the positive deadtime switching state $+D_t$, and the freewheeling switching state Z_v, and N_M includes the negative voltage switching state N_v, the negative deadtime switching state $-D_t$, and Z_v. Between P_M and N_M, there is a mode transition deadtime D_t.

As shown in Fig. 2(a), when the HERIC inverter operates at P_M (i.e., $v_{ref} > 0$), S_5 is ON, and $S_{1,4}$ and S_6 switch at a high frequency (i.e., changing between P_v and Z_v). The deadtime (i.e., $+D_t$) should be inserted between the switching of $S_{1,4}$ and S_6, where S_5 is ON, and the rest switches are OFF. While the HERIC inverter works at N_M (i.e., $v_{ref} < 0$), S_6 is ON, and

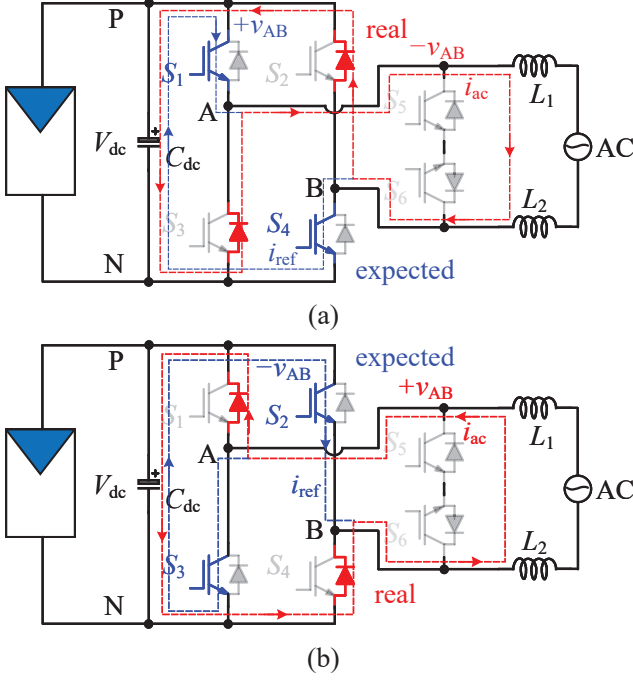| v_{ref}	State	S_1	S_2	S_3	S_4	S_5	S_6	Transition	State	S_1	S_2	S_3	S_4	S_5	S_6
P_M	+**Dt**	−	−	−	−	+	−	T_{NP}	**Dt**	−	−	−	−	−	−
	Pv	+	−	−	+	−	+		**Pv**	+	−	−	+	−	+
	+**Dt**	−	−	−	−	+	−		+**Dt**	−	−	−	−	+	−
	Zv	−	−	−	−	+	+		**Zv**	−	−	−	−	+	+
N_M	−**Dt**	−	−	−	−	−	+	T_{PN}	**Dt**	−	−	−	−	−	−
	Nv	−	+	+	−	−	+		**Nv**	−	+	+	−	−	+
	−**Dt**	−	−	−	−	−	+		−**Dt**	−	−	−	−	−	+
	Zv	−	−	−	−	+	+		**Zv**	−	−	−	−	+	+

Fig. 3. Voltage performance during mode transitions with unthorough transition method, (a) P_M and (b) N_M.

$S_{2,3}$ and S_5 change at a high frequency (i.e., changing between N_v and Z_v). Between the switching of $S_{2,3}$ and S_5, there is a deadtime interval (i.e., $-D_t$), in which only S_6 is ON. Besides, D_t between P_M and N_M disconnects all the switches $S_{1\text{-}6}$, as shown as the red part in Fig. 2.

B. Distortion analysis

This paper only focuses on the effects caused by the deadtime during the operation mode transition zone. The ideal modulation signal v_{ref} is depicted as the red dotted line in Fig. 2(b), generating the reference AC output current i_{ref} (see blue dotted line in Fig. 2(b)). However, there always exists the polarity fluctuation of the real modulation signal v_m at the zero-cross point due to the measurement noise and the deadtime state. In that case, the traditional transition strategy with the deadtime described in [11] always leads to the current distortion at this zone, as illustrated as the red solid line in Fig. 2(b). In particularly, when the inverter output negative

power (i.e, v_{AC} is reversed to i_{AC}), the distortion is more amplified due to the uncontrolled current path in the deadtime interval. As shown in Fig. 3 (a) and (b), the blue current path is the expected, where $S_{1,4}$ and $S_{2,3}$ should be ON at P_M and N_M, respectively. However, the real current flows through the body diodes of $S_{2,3}$ and the body diodes of $S_{1,4}$, respectively, as the red dotted line in Fig. 3, where the inverter output the opposite voltage of the expected one. In that case, the current distortion happens due to the polarity fluctuation of v_m, as depicted as i_{ac} (the blue solid line) in Fig. 2(b).

III. PROPOSED MODE TRANSITION STRATEGY

To improve the current distortion during the zero-cross zone of v_m, an improved operation mode transition method is proposed to reduce the distortion as well as avoid the short-circuit issue. First of all, two extra operation modes are introduced to ensure the smooth transition, as shown in Table. II. The first mode is T_{NP}, which is when v_m changes from the negative half-cycle to the positive half-cyle, including four switching states P_v, $+D_t$, Z_v and D_t. The other is T_{PN}, which is when v_m switches from the positive half-cycle to the negative half-cyle, containing four switching states N_v, $-D_t$, Z_v and D_t. All four operation modes (i.e., P_M, N_M, T_{NP} T_{NP}) are depicted in Table II.

Accordingly, the proposed operation mode transition strategy is shown in Fig. 4. There is a two-level judgment to decide the operation mode in the next switching period. Both the current modulation voltage v_m and the operation mode at the last period are used for the judgment. When $v_m \geq 0$, the current mode will be P_M if the last mode is OFF, P_M. Otherwise, the current should be T_{NP} if the last mode is N_M and T_{PN}. This judgment is similar when $v_m < 0$, as shown in Table. II, where the current mode is N_M if the last mode is OFF, N_M, and the current mode is T_{PN} if the last mode is P_M and T_{NP}. If all the four conditions of the last mode are not met, the current mode is OFF, in which all switches $S_{1\text{-}6}$ are disconnected.

With the proposed operation mode transition strategy, the transition can be ensured successfully and the zero-cross distortion can be improved. The contribution is that the proposed method adopts two-level judgment, which is better than the traditional one (i.e., judging operation transitions only by v_m)
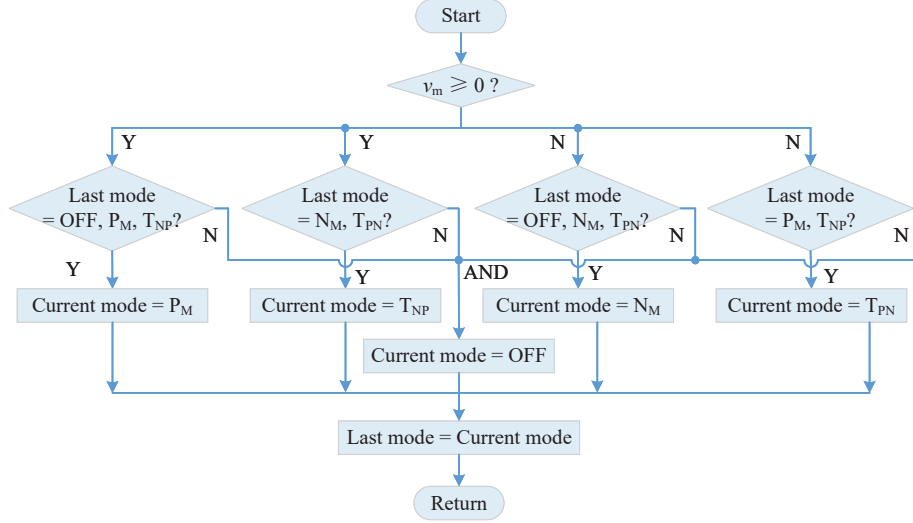
Fig. 4. Proposed operation mode transition strategy, where 'AND' means the AND judgment for all 'N' conditions of the last mode.

IV. SIMULATION AND EXPERIMENTAL RESULTS

To verify the performance of the proposed transition scheme, simulations and experimental tests are carried out on an down-scaled HERIC inverter, where the parameters are $V_{dc} = 50$ V, $v_{ac} = 31$ V/ 50 Hz, $C_{dc} = 1000$ uF, and $L_1 = L_2 = 0.75$ mH. The PV port is connected to a constant DC power source 1, and the AC port is connected to the utility grid by a voltage regulator, respectively. The following compares the traditional transition method and the proposed operation mode transition strategy under the conditions of the oscillated sampling AC voltage v_{AC} during the zero-cross point. The switching frequency is 20 kHz, and the deadtime is set as 1 us in both transition methods.

The simulation results are shown in Fig. 5, where the power factor is 0, and the inverter only outputs reactive power. v_{AB} is the modulation voltage before the AC filters, v_{AC} is the inverter output voltage, and i_{AC} is the AC current. As shown in Fig. 5(a), the total harmonic distortion (THD) of i_{AC} with the unthorough mode transition method is 6.66 %, which is higher than the required value (i.e., 5 %) for the grid-connected inverter standard [7]. As shown as the zoom-in part in Fig. 5 (a), v_{AB} has a large and longtime fluctuation during the zero-cross interval of v_m, where v_{AB} changes among $+V_{dc}$, $-V_{dc}$ and 0 at a high frequency. The distortion in Fig. 5(a) agrees well with the distortion analysis in Section II. By comparison, the THD shown in Fig. 5(b) is 2.01 % with the proposed mode transition method. It is validated in Fig. 5 that the proposed operation mode transition operation strategy can ensure reliable mode transition and high power quality.

In addition, Fig. 6 shows the experimental tests, where the power factor is -1 and the inverter output negative power. As shown in Fig. 6 (a), there is distortion during the transition zone, where v_{AB} has a large and longtime fluctuation. The THDs in Fig. 6(a) and (b) are 5.8 % and 2.6 %, respectively, which means that the proposed transition method can effec-
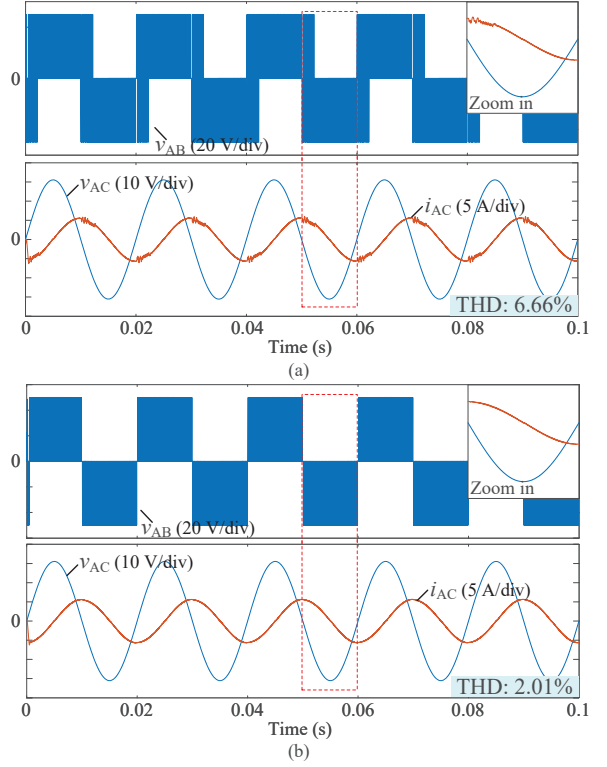

Fig. 5. Simulation results, (a) un-thorough transition method and (b) proposed transition strategy, where v_{AB}, v_{ac} and i_{ac} are the modulation voltage, the grid voltage, and the grid current, respectively.

tively alleviate the zero-cross distortion. The comparison results agree well with the simulation and the distortion analysis. Both the simulation and experimental tests consistently verify that the proposed transition scheme can effectively improve the performance in terms of the power quality of the grid current during the operation mode transition zone.
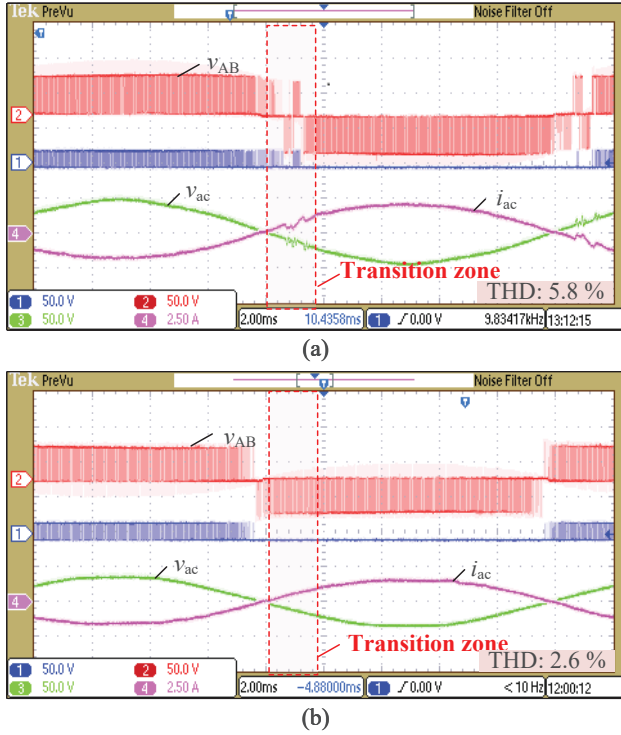
Fig. 6. Experimental results of the mode transition method comparison, (a) un-thorough transition method and (b) proposed transition strategy.

V. Conclusion

This paper proposed an improved operation mode transition strategy. In this strategy, two additional transition operation modes are employed to ensure short-circuit protection as well as the expected voltage output. Then, the operation mode transition strategy is designed through a two-level judgment to achieve a safe mode transition. The proposed strategy with enhanced performance during the mode transition can effectively improve the current distortion in the zero cross period. Simulations and experimental results have validated the good power quality of the grid current in the proposed strategy even under the condition of reactive power injection. The proposed transition method can be employed in most transformerless single-phase inverters with the reactive power injection modulation method.

References

[1] Rajiv K. Varma, "Smart solar PV inverters with advanced grid support functionalities-Chapter: impacts of high penetration of solar PV systems and smart inverter developments," *Wiley-IEEE Press*, 2022, pp.1–34.

[2] S. Kouro, J. I. Leon, D. Vinnikov and L. G. Franquelo, "Grid-Connected Photovoltaic Systems: An overview of recent research and rmerging PV converter technology," *IEEE Ind. Electron. Mag.*, vol. 9, no. 1, pp. 47–61, Mar. 2015.

[3] Y. Chen and D. Xu, "Review of soft-switching topologies for single-phase photovoltaic inverters," *IEEE Trans. Power Electron.*, vol. 37, no. 2, pp. 1926–1944, Feb. 2022.

[4] Z. Tang, Y. Yang and F. Blaabjerg, "Power electronics: The enabling technology for renewable energy integration, " *CSEE J. Power Energy Syst.*, vol. 8, no. 1, pp. 39–52, Jan. 2022.

[5] R. Dogga and M. Pathak, "Recent trends in solar PV inverter topologies," *Solar Energy*, vol. 183, pp. 57–73, May 2019.

[6] Z. Tang, A. Sangwongwanich, Y. Yang, and F. Blaabjerg, "Energy efficiency enhancement in full-bridge PV inverters with advanced modulations," *e-Prime*, p. 100004, Oct. 2021.

[7] IEEE Standard Committee, *IEEE standard for interconnection and interoperability of dis-tributed energy resources with associated electric power systems interfaces*, IEEE Std 1547–2018 Std., Apr 2018.

[8] T. Wu, C. Kuo, K. Sun and H. Hsieh, "Combined unipolar and bipolar PWM for current distortion improvement during power compensation," *IEEE Trans. Power Electron.*, vol. 29, no. 4, pp. 1702–1709, Apr. 2014.

[9] T. K. S. Freddy, J.-H. Lee, H.-C. Moon, K.-B. Lee, and N. A. Rahim, "Modulation technique for single-phase transformerless photovoltaic inverters with reactive power capability," *IEEE Trans. Ind. Electron.*, vol. 64, no. 9, pp. 6989–6999, 2017.

[10] Z. Ahmad and S. Singh, "An improved single phase transformerless inverter topology for grid connected PV system with reduce leakage current and reactive power capability," *Solar Energy*, vol. 157, pp. 133–146, Nov. 2017.

[11] B. Weber, T. Brandt and A. Mertens, "Compensation of switching dead-time effects in voltage-fed PWM inverters using FPGA-based current oversampling," *Proc. APEC 2016*, pp. 3172–3179, Mar. 2016.

[12] Y. Yang, K. Zhou, H.Wang, and F. Blaabjerg, "Analysis and mitigation of dead-time harmonics in the single-phase full-bridge pwm converter with repetitive controllers, " *IEEE Trans. Ind. Appli.*, vol. 54, no. 5, pp. 5343–5354, 2018.

[13] Z. Tang, Y. Yang, M. Su, T. Jiang, F. Blaabjerg, H. Dan, and X. Liang, "Modulation for the avc-heric inverter to compensate for deadtime and minimum pulsewidth limitation distortions," *IEEE Trans. Power Electron.*, vol. 35, no. 3, pp. 2571–2584, 2020.